Modification of Ti-6Al-4V titanium alloy surface relief by compression plasma flows impact

Nikolai Cherenda [1]*, Artem Leivi [2], Alexandra Petuh [1], Vladimir Uglov [1], Sergey Grigoriev [3], Alexey Vereschaka, Valentin Astashinski [5], Anton Kuzmitski [5]

[1]Belarusian State University, Nezavisimosti ave. 4, 220030 Minsk, Belarus; cherenda@bsu.by (N.C.), alya.petukh.01@mail.ru (A.P.), uglov@bsu.by (V.U.)
[2]Federal State Autonomous Educational Institution of Higher Education "South Ural State University (national research university), 76, Lenin prospekt, Chelyabinsk, Russia, 454080; leiviai@susu.ru
[3]Moscow State University of Technology "STANKIN", Vadkovsky Lane 3a, 127055 Moscow, Russia; s.grigoriev@stankin.ru
[4]Institute of Design and Technological Informatics of the Russian Academy of Sciences (IDTI RAS), Vadkovsky Lane 18a, 127055 Moscow, Russia; dr.a.veres@yandex.ru
[5]A.V.Lykov Heat and Mass Transfer Institute of the National Academy of sciences of Belarus, P. Brovka str. 15, 220072 Minsk, Belarus; ast@hmti.ac.by (V.A.), antey@hmti.ac.by (A.K.)
*Correspondence: cherenda@bsu.by

Abstract: Investigation of compression plasma flows impact on surface relief of Ti-6Al-4V titanium alloy was carried out in this work. Profilometry, X-ray diffraction, scanning electron microscopy and samples weight measurements were used as investigation techniques. The findings showed that plasma impact led to the formation of developed surface relief (R_a parameter was changed in the range of 0.7-2.7 μm) due to the action of hydrodynamic instabilities at the melt-plasma border. Increase in the number of pulses resulted in the growth of R_a value. Numerical simulation of surface evolution under plasma impact was carried out on the basis of the model of incompressible fluid potential flow. Simulation data correlated with experimental data set. The hydrodynamic flow of the melt during plasma impact led to another process - surface erosion. Increase in both the absorbed energy density and the number of pulses resulted in erosion intensity increase. Formation of titanium nitride on the surface was observed as a result of the interaction of nitrogen (as a plasma generating gas) with the surface heated under plasma impact. Titanium nitride film prevented the development of the surface relief formed by the action of hydrodynamic instabilities.

Keywords: titanium alloy; medical implants; plasma; hydrodynamic instabilities; surface relief; phase composition; erosion; titanium nitride

1. Introduction

Metallic materials started to be used as medical implants from 19th century at least (Chen and Thouas, 2015). The main requirements for metallic implants are: biocompatibility, corrosion resistance, suitable mechanical properties (including wear resistance) and good osseo-integration (Chen and Thouas, 2015). Titanium and its alloys satisfy most of these requirements that is why this group of metallic materials is widely used for medical implants production (Chen and Thouas, 2015; Nouri and Wen, 2015). Titanium and its alloys possess good mechanical properties, excellent corrosion resistance, low density, their Young's modulus is less that of stainless steel and Co-Cr alloys (Chen and Thouas, 2015; Nouri and Wen, 2015; Khorasani et.al., 2015; Chouirfa et.al., 2019; Wang, 2020; Kaur and Singh, 2019). But titanium is poor in tribological properties (Chen and Thouas, 2015).

Ti-6Al-4V is one of the most widely used titanium alloy for orthopedic and dental applications (Brunello et.al.; 2018). It is a typical α+β type alloy with good combination of corrosion resistance and mechanical properties. At the same time it was reported that the first generation of these alloys caused allergic reactions in the human body (Chen and Thouas, 2015). Besides that it contains potentially toxic atoms of aluminum and vanadium (Chen and Thouas, 2015; Nouri and Wen, 2015; Khorasani et.al., 2015; Kaur and Singh, 2019; Chen et.al., 2023) which have the risk of releasing into the human body. It should be noted that harmful influence of these elements was observed after absorption by human body in very high doses (Chen and Thouas, 2015). There are several ways to avoid this negative effect. The most common are: development and usage of new Ti based alloys that have little or no toxic elements in composition and application of different surface modification techniques e.g. protective coatings deposition. The last approach will be considered below. In (Nouri and Wen, 2015; Chen et.al., 2023) it was reported on

development of Ti-Nb-Zr, Ti-Zr-Nb-Me (Me-metal), Ti-Sn-Nb, Ti–Nb–Zr–Si and Ti-Ni-Ta alloys for biomedical applications. A large number of investigations in this direction concerns Ti-Cu alloys (Lu et.al., 2021; Liu, 2020; Zhang et.al., 2021). Ti–Cu alloys showed potential application in clinical field due to their excellent antibacterial properties, good corrosion resistance and mechanical properties, osteogenic ability in vivo and in vitro (Lu et.al., 2021; Liu, 2020; Zhang et.al., 2021).

The texture and roughness of titanium based implants surface is one of the crucial factors determining the biological performance (Khorasani et.al., 2015; Zhang et.al, 2021; Lüdecke et.al., 2013; Lu et.al., 2020; Truong et.al., 2010; Robles et.al., 2023; Yang et.al., 2022). Surface roughness influences the protein adsorption, the cell response, the tissue adhesion as well as the adhesion of microorganisms, wear behavior, adhesion of protective coatings etc. (Khorasani et.al., 2015; Zhang et.al, 2021; Lüdecke et.al., 2013; Lu et.al., 2020; Truong et.al., 2010; Robles et.al., 2023; Yang et.al., 2022; Padmini et.al., 2020; Takadoum and Bennani; 1997). Three levels of surface morphology are usually discussed: nano-scale, micro-scale and macro-scale (Wang et.al., 2020). Many researchers found that surface roughness on nano-meter scale has strong influence on bacterial adhesion (Zhang et.al, 2021; Lüdecke et.al., 2013; Lu et.al., 2020; Truong et.al., 2010; Robles et.al., 2023; Yang et.al., 2022). It is considered that bacterial surface coverage decreases with increasing roughness on a nano-scale (Lüdecke et.al., 2013; Lu et.al., 2020; Yang et.al., 2023). In (Lu et.al., 2020) it was shown that number of adherent bacteria on the surface with a roughness of R_a=1 nm is only 2% of that on a ground surface with a surface roughness of R_a=205 nm. The same tendency was found in (Yang et.al., 2023): bacteria prefer to adhere on the smoother surface under static culture conditions than at the surface with R_a in the range of 0.23-6.13 nm. The main reason of this effect is the weakening of adhesion force due to decrease of the contact area between bacteria and surface (Yang et.al., 2023). At the same time in (Truong, et.al.; 2020) it was found that different bacteria revealed different behavior with roughness change.

Micro-scale morphology also can influence bacterial adhesion. But bacterial adhesion properties are different in nano-scale and micro-scale levels (Yang et.al., 2023). It was reported that the bacteria adhesion force to surface increasing with the growth of the roughness at sub-micro or micro- scale level, until the critical value of roughness is reached (Yang et.al., 2023). Thus one can see that roughness at nano-scale level provides best anti-adhesion property while micro-scale roughness promotes bacterial adhesion. For smooth surfaces bacteria adhesion is mainly depends on other material properties (Yang et.al., 2023).

Osseo-integration as a fundamental requirement for implants is strongly dependent on surface morphology on a micro-scale level (Wang et.al., 2020; Robles et.al., 2023; Aparicio et.al., 2011; Kurup et.al., 2021). A developed surface improves mechanical contact with surrounding tissues due to the ingrowth of bone tissue into the formed relief. It has been observed that a surface with micron roughness promotes faster bone healing (Wang et.al., 2020; Robles et.al., 2023; Aparicio et.al., 2011; Tardelli et.al., 2022). The roughness value in the range of 1-10 μm provides best conditions for osseo-integration of titanium implants (Robles et.al., 2023; Tardelli et.al., 2022).

Surface roughness also influences on adhesion of protective coatings to implants surface. In general, increase in the surface roughness should lead to the growth of interface area between coating and substrate and hence to the growth of number of bonds and growth of adhesion force (Croll, 2020). Adhesion force increase was observed e.g. in (Bruera, 2023) for cold-sprayed Cu particles deposited on stainless steel substrate with the growth of roughness up to a R_z ~ 34 μm. A roughened surface also can increase adhesion force due to overcoming the external force during peeling adhesion test (Croll, 2020). At the same time there are examples that increase of surface roughness both at nano- and micro-scale level resulted in coating adhesion decrease (diminishing of a critical load necessary for coating delamination) (Takadoum and Bennani, 1997; Bruera et.al., 2023). It should be noted that critical load determined in adhesion tests depends on many factors (Steinmann et.al., 1987). All of these factors including surface roughness should be analyzed thoroughly for revealing correct regularities.

A number of techniques have been used for implant surface modification just to prevent bacterial attachment, enhance osseo-integration, increase mechanical and tribological properties, etc. (Nouri and Wen, 2015; Chouirfa et.al., 2019; Wang et.al, 2020; Lu et.al., 2020; Kurup et.al., 2021; Herrera-Jimenez et.al., 2021; Simões et.al., 2023; Grabovetskaya et.al., 2023; Wu et.al., 2023; Sachin et.al., 2022). According to (Nouri and Wen, 2015) metallic materials surface modification techniques can be divided on two main groups: physicochemical and biochemical treatments. Techniques based on treatments impacting morphology belong to the first group: grit blasting, abrading, electro-erosion, acidic or alkaline treatments, physical and electrochemical deposition etc. (Nouri and Wen, 2015; Chouirfa et.al., 2019; Kaur and Singh, 2019). Such techniques as conjugation of biological molecules to mimic biointerfaces, covering by antibiotics and antimicrobial peptides etc. compose the second group (Nouri and Wen, 2015; Chouirfa et.al., 2019). However, many of these techniques can be interconnected. A large group of comparatively new implant surface modification techniques based on ions (Khorasani et.al, 2015; Lu et.al., 2020; Wu et.al., 2023), electrons (Grabovetskaya et.al., 2023; Robles et.al., 2023), laser (Grabovetskaya et.al., 2023; Robles et.al., 2023; Simões et.al., 2023) and plasma (Chouirfa, 2019; Truong et.al., 2020; Herrera-Jimenez et.al., 2021) treatment is developing last decades. It should be noted that surface modification techniques are mainly applied for mounting surfaces (bonding surface with a body tissue) of the joint implants, and are not suitable for bearing surfaces (Lu et.al., 2020). More detailed analysis and classification of metal implants surface modification techniques can be find in (Chouirfa et.al., 2019; Wang et.al., 2020; Chen et.al., 2023; Robles et.al., 2023; Wu et.al., 2023; Sachin et.al., 2022).

Compression plasma flows (CPF) generated by quasi-stationary plasma accelerators can be also effectively used for modification of Ti-6Al-4V titanium alloy surface (Cherenda et.al., 2018). It was shown that plasma impact resulted in diminishing of toxic elements (Al and V) concentration at the surface. CPF treatment of the target led to the surface layer melting; initiation of hydrodynamic instabilities and appearance of convection mass and heat transfer flows in the melt and disturbance of the melt surface; crystallization in conditions of superfast cooling of the melt (up to 10^7 K/s) after the end of plasma pulse (Astashynski et.al., 2014; Cherenda et.al., 2018). Developed surface relief is formed after treatment as a result (Astashynski et.al., 2014). Short literature review showed that surface relief is strongly influences on exploitation properties of medical implants. Thus investigation of the influence of CPF treatment parameters on surface roughness as well as analysis of the physical processes occurred during plasma impact on Ti-6Al-4V titanium alloy was the aim of this work.

2. Experimental

The samples of Ti-6Al-4V titanium alloy (Grade 5) were used for investigations. The diameter of the samples was 25 mm, their thickness – 3 mm. The samples were mechanically grinded before plasma treatment.

Compression plasma flows were obtained using a gas-discharge quasi-stationary plasma accelerator: magneto-plasma compressor (MPC) of compact geometry powered with the capacitive storage of 1200 mF, operating at the voltage of 4 kV. Nitrogen was used as a plasma-forming gas. The pressure in the pre-evacuated vacuum chamber was 10^{-3} Pa. The pressure of plasma-forming gas was 400 Pa. The discharge duration in the MPC amounts to 100 μs. The physical principles of CPF generation are as follows. Following the interelectrode gap breakdown, the generated plasma is accelerated in the discharge device by the Ampere force and outflows from the discharge unit. The length of the plasma flow is about 10-12 cm. In the zone of maximum contraction it constitutes 1 cm in diameter. The compression of the plasma flow takes place due to the interaction of the longitudinal component of the discharge current 'swept away' from the discharge device with the intrinsic azimuth magnetic field. The plasma velocity in the compression flow amounts to $(4–7)\cdot10^6$cm/s, depending on the initial parameters of acceleration. The concentration and temperature of electrons in the field of maximum contraction reach (1–10) 10^{17} cm^{-3} and 1–3 eV. The peculiarities of the plasma accelerator construction, principles of plasma flows generation and scheme of the discharge device can be found in (Uglov, 2002).

The energy absorbed by the surface layer of the target is dependent on the distance between the sample and the cathode, the bank capacitor initial voltage, the pressure of nitrogen in the vacuum chamber and the number of pulses. In these series of experiments the distance between the sample and the cathode was changed in the range of 14-8 cm corresponding to the energy density absorbed by the surface layer (Q) 26-43 J/cm^2 per pulse (registered by calorimetric measurements). Treatment was carried out by 1-6 pulses (n) at the interval of 3-5 s.

Surface topography was characterized using MarSufr SD 26 profilometer. Six tracks were made on each of the sample. The length of the track was 17 mm, length of base line for calculation of roughness and waviness parameters was 5.7 mm. Each parameter was averaged after measurements on 6 tracks. The samples weight was determined before and after CPF treatment by analytical balance RADWAG AS 60/220/C/2/N with the accuracy of ±0.05 mg. The phase composition of the surface layer was investigated by means of the X-ray diffraction method using the Ultima IV RIGAKU diffractometer in Bragg-Brentano geometry with parallel beams in Cu Kα radiation. The surface morphology of the samples was also studied using scanning electron microscopy (SEM) on a LEO1455VP microscope combined with an Oxford X-ray detector for energy-dispersion X-ray microanalysis.

3. Results and Discussion

3.1. Surface topography

The results of surface roughness and waviness parameters investigation are presented in Figure 1. In the initial state, before plasma treatment, the parameters of the surface roughness and waviness were equal to: R_a=0.4 μm, R_z=4.1 μm, R_{max}=5.9 μm, W_a= 0.24 μm. The CPF impact led to the formation of a more developed surface (Figure 1). In particular, in the used range of treatment regimes, the R_a parameter was increased up to 2.7 μm, R_z - up to 16 μm, R_{max} - up to 26.5 μm, and W_a - up to 5.2 μm. One can see that R_a value corresponds to the roughness range providing best conditions for osseo-integration (Robles et.al., 2023; Tardelli et.al., 2022). Figure 1 shows that the increase in the number of pulses for Q=30-43 J/cm^2 resulted in the growth of R_a value. During treatment with minimal Q value of 26 J/cm^2 R_a was almost independent on the number of pulses and was changed in the region of 1.2–1.45 μm. Such behavior is associated with a significant change in the composition of the surface layer during plasma impact and will be discussed later. No clear dependence of Ra on the energy absorbed by the surface layer can be finding. For example, an increase in the absorbed energy from 30 to 43 J/cm^2 led to the Ra growth after CPF treatment by 1 and 3 pulses, while at 6 pulses the maximum R_a value was observed at 37 J/cm^2.

R_z and R_{max} parameters were also increased with the growth of pulses number for absorbed energy density of 37 J/cm^2 (Figure 1 b and c). For other Q values a large scatter of data was obtained for these parameters that do not allow revealing unambiguous regularities. It should be noted that the R_a parameter was estimated and averaged over more number of points than the R_z and R_{max} parameters (by definition). Therefore, under conditions of a developed surface formed by CPF it is necessary to increase the amount of data, i.e. the number of tracks being taken in order to obtain statistically reliable dependences of these parameters on the treatment regimes. The behavior of the waviness parameter W_a correlates with the behavior of R_a (Figure 1d). W_a was increased from 1.4 to 5.2 μm with the growth of pulses number and the absorbed energy density.

When solid targets are exposed to intense particles and plasma beams, a significant change in the relief of the irradiated surface is observed. The final surface relief depends on many factors: the initial surface relief, processing modes (absorbed energy density, number of pulses, pulse duration), and properties of the target material itself (Astashinski et.al., 2014; Krasnikov et.al., 2007). Surface layer of the solid targets is melted under high-energy impact. The surface of the melt can acquire an acceleration of the order of 10^8-10^{11} m/s^2 due to energy and impulse transfer from the beam (Astashinski et.al., 2014; Krasnikov et.al., 2007). Such hydrodynamic flow of the melt is one of the key factors determining the formation of the

resulting surface relief under high-temperature plasma treatment due to appearance of hydrodynamic instabilities at the plasma – melt border (Chandrasekhar, 1961; Bazylev et.al., 2009; Konovalov et.al., 2017; Nevskii et.al., 2020; Sarychev et.al., 2010). Necessary conditions for instabilities formation are realized during CPF treatment (Astashinski et.al., 2014). As a result the plasma-melt interface will be modulated (that is, changes shape) due to a sharp increase in the amplitude of initially small perturbations. Such perturbations begin to increase with time and, after crystallization, determine mainly the surface topography.

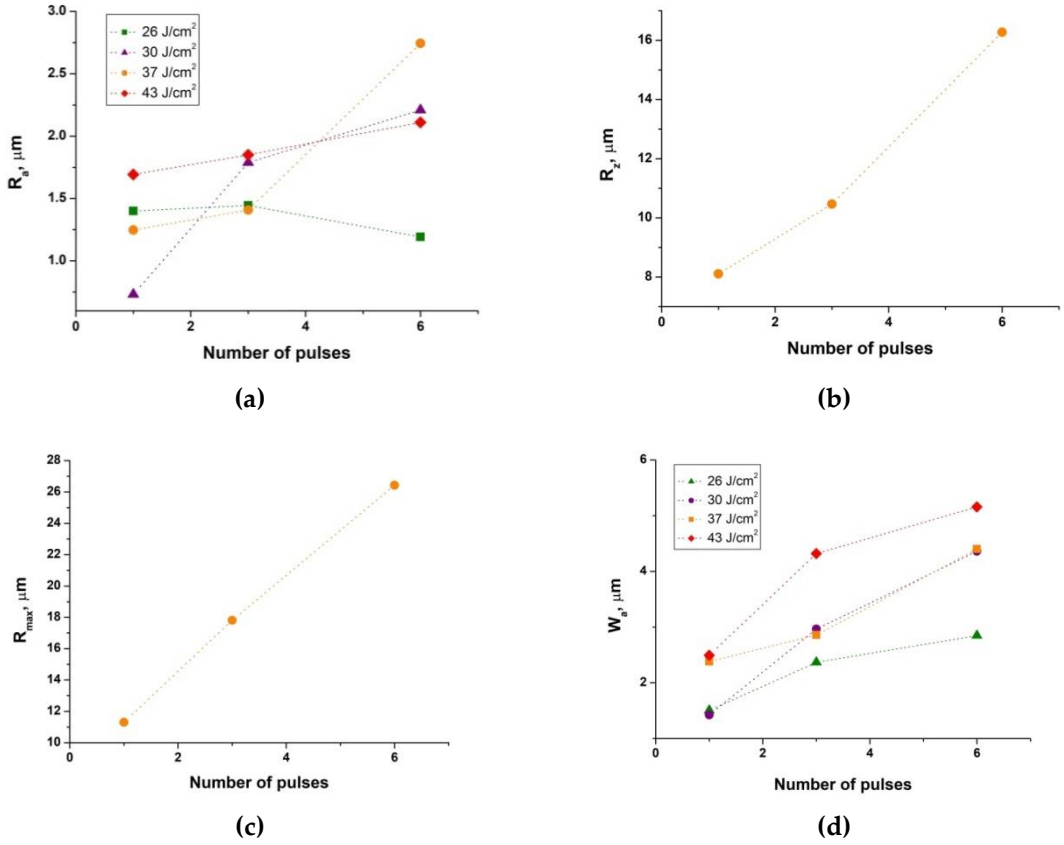

Figure 1. Dependence of R_a (a), R_z (b), R_{max} (c), W_a (d) on CPF treatment regimes.

After disintegration of the plasma pulse, the melted layers move by inertia. In this case, the dynamics of the target surface is determined by the balance of surface tension forces, inertia forces caused by the accelerated movement of the target surface layer and viscous forces. Under the action of surface tension forces the perturbed target surface begins to experience oscillations (capillary waves). The presence of viscous forces leads to dissipation of the energy of vibrations and to their damping, as a result of which the amplitude of perturbations decreases. The inertia forces possess destabilizing character in general.

Under the conditions of this experiment, an increase in the density of the energy absorbed by the surface time led to an increase in the lifetime of the melt. This means that the perturbations sizes and roughness and waviness parameters as well should be larger. As the number of impulses increases, each subsequent impulse is superimposed on a more developed surface created by the previous impulse, that is, it creates an increasingly developed surface. Thus, the observed regularities of surface roughness and waviness changes on the absorbed energy density and the number of pulses can be qualitatively explained from the point of view of the onset and development of the hydrodynamic instabilities at the plasma-melt interface under the action of the CPF.

3.2. Numerical simulation of surface topography

The model of the potential flow of an incompressible fluid described in (Krasnikov et.al., 2007) taking into account hydrodynamic instabilities was used to simulate the relief of the Ti surface under CPF impact. Let's direct the axis z deep into the target, and the axes x and y - along the surface (Figure 2). In the unperturbed state, the target surface is considered to be a plane.

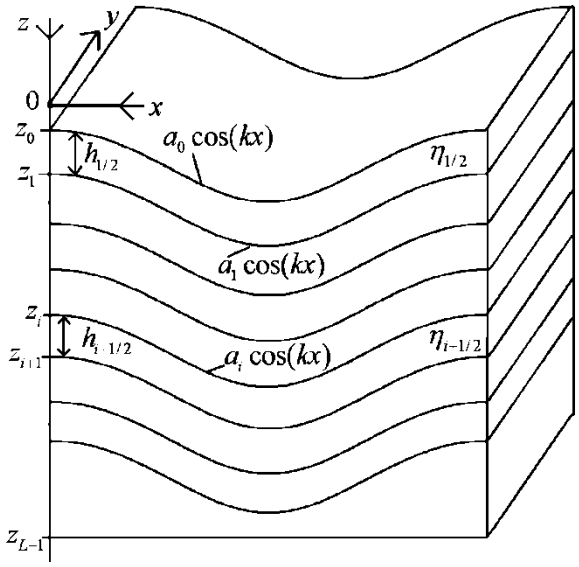

Figure 2. Dynamics of the multilayered medium – geometry of the problem.

According to this model, an inhomogeneous in volume medium is considered as a multilayer one. The following system of equations for describing the dynamics of the surface of a multilayer target can be written (Krasnikov et.al., 2007):

$$\beta_{i-1/2}\ddot{a}_{i-1}+\beta_i\ddot{a}_i+\beta_{i+1/2}\ddot{a}_{i+1}=\alpha_{i-1/2}a_{i-1}+(\alpha_i-k^2\sigma_i)a_i+\alpha_{i+1/2}a_{i+1}-$$
$$-(\gamma_{i-1/2}+\dot{\beta}_{i-1/2})\dot{a}_{i-1}-(\gamma_i+\dot{\beta}_i)\dot{a}_i-(\gamma_{i+1/2}+\dot{\beta}_{i+1/2})\dot{a}_{i+1},\quad i=0,L-1,\ \text{where}$$

$$\beta_i=\frac{1}{4k}\frac{1}{\operatorname{sh}^2\left[kh_{i-1/2}\right]}\left[\int_0^{h_{i-1/2}}\rho_0(z_{i-1}+\xi)\,de^{+2k\xi}+\int_0^{h_{i-1/2}}\rho_0(z_{i-1}+\xi)\,de^{-2k\xi}\right]+$$
$$+\frac{1}{4k}\left(1-\operatorname{cth}\left[kh_{i+1/2}\right]\right)^2\int_0^{h_{i+1/2}}\rho_0(z_i+\xi)\,de^{+2k\xi}+\frac{1}{4k}\left(1+\operatorname{cth}\left[kh_{i+1/2}\right]\right)^2\int_0^{h_{i+1/2}}\rho_0(z_i+\xi)\,de^{-2k\xi},$$

$$\beta_{i+1/2}=\frac{1}{4k}\frac{1}{\operatorname{sh}\left[kh_{i+1/2}\right]}\times$$
$$\times\left[\left(1-\operatorname{cth}\left[kh_{i+1/2}\right]\right)\int_0^{h_{i+1/2}}\rho_0(z_i+\xi)\,de^{+2k\xi}-\left(1+\operatorname{cth}\left[kh_{i+1/2}\right]\right)\int_0^{h_{i+1/2}}\rho_0(z_i+\xi)\,de^{-2k\xi}\right].$$

$$\gamma_i=4k\left\{\eta_{i-1/2}\operatorname{cth}\left[kh_{i-1/2}\right]+\eta_{i+1/2}\operatorname{cth}\left[kh_{i+1/2}\right]\right\}$$

$$\gamma_{i+1/2}=4k\left\{-\frac{\eta_{i+1/2}}{\operatorname{sh}\left[kh_{i+1/2}\right]}\right\}$$

$$\alpha_i(k,t)=\int_{z_{i-1}}^{z_i}\left(\frac{\operatorname{sh}\left[k(z-z_{i-1})\right]}{\operatorname{sh}\left[kh_{i-1/2}\right]}\right)^2 g(z)\frac{\partial\rho_0(z,t)}{\partial z}dz+$$
$$+\int_{z_i}^{z_{i+1}}\left[\operatorname{ch}\left[k(z-z_i)\right]-\operatorname{sh}\left[k(z-z_i)\right]\operatorname{cth}\left[kh_{i+1/2}\right]\right]^2 g(z)\frac{\partial\rho_0(z,t)}{\partial z}dz,$$

$$\alpha_{i+1/2}(k,t)=\int_{z_i}^{z_{i+1}}\left[\operatorname{ch}\left[k(z-z_i)\right]-\operatorname{sh}\left[k(z-z_i)\right]\operatorname{cth}\left[kh_{i+1/2}\right]\right]\frac{\operatorname{sh}\left[k(z-z_i)\right]}{\operatorname{sh}\left[kh_{i+1/2}\right]}g(z)\frac{\partial\rho_0(z,t)}{\partial z}dz$$

where $a_{-1} = 0$ - vacuum area over the target, $a_L = 0$ - stationary bottom of the molten pool, $\eta_{i+1/2}$ - coefficient of dynamic viscosity of the layer with number $i+1/2$, $h_{i+1/2} = z_{i+1} - z_i$ - thickness of the layer with the number $i+1/2$, σ_i - coefficient of the surface tension of the corresponding border between layers.

This system of equations makes it possible to describe the evolution of small perturbations on the background of the known one-dimensional motion of matter flow (including the dynamics of the target surface topography) from known distributions of density $\rho(z,t)$ and acceleration $g(z,t)$. The resulting system of equations is also valid for perturbations of the $z(x,y,t) = a(t)\cos(k_x x)\sin(k_y x)$ form, where $k = \sqrt{k_x^2 + k_y^2}$, and also for perturbations of the $z(r,t) = a(t)J_0(kr)$ form, where J_0 is the zero-order Bessel function. The calculation of the thermodynamic parameters of a substance under the influence of a CPF was carried out using the BETAIN software package (Leyvi, 2017).

The results of numerical simulation are presented in Figure 3. The target surface is shown before and after the CPF impact. It can be seen from the figure that, on the one hand, the roughness of the target was increased, and, on the other hand, the short-wavelength part of the perturbation is damped.

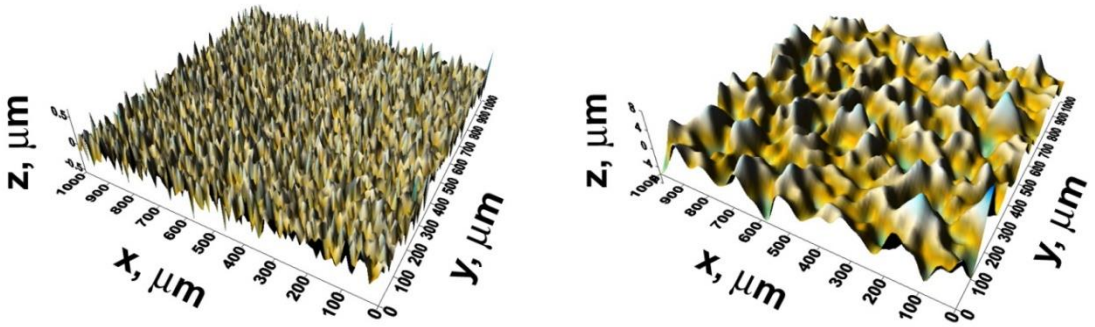

(a) **(b)**

Figure 3. Ti surface before (a) and after one pulse of CPF impact at Q=37 J/cm^2 (b).

Let us consider results of numerical simulation of the target surface for samples treated by CPF with 1 and 3 pulses at Q=37 J/cm^2. Simulation was carried pulse by pulse taking into account change of surface relief after each pulse. The surface relief z(x,y) was simulated and accidental surface profile in (x,y) plane was taken from calculated data. The comparison between experimental and simulated surface profiles is shown in Figure 4.

One can see from Figure 4 that correlation between simulated and experimental data is observed. An increase of pulses number resulted in a smoothing of the short-wavelength part of the surface relief and growing of the long-wavelength part. That is, the roughness increases. This is due to the fact that with an increase in the number of pulses, the time of existence of the melt pool increases, respectively, the short-wavelength part is smoothed out better. The presence of viscous forces leads to dissipation of the perturbations energy and to their damping. The amplitude of perturbations decreases, as a result. Similar results are valid as the input energy density increases. In this case, an increase in the lifetime of the melt pool is also observed; accordingly, the short-wavelength part of the harmonics will be smoothed out.

It should be noted that the numerical model does not take into account changes in roughness associated with the processes of substance crystallization.

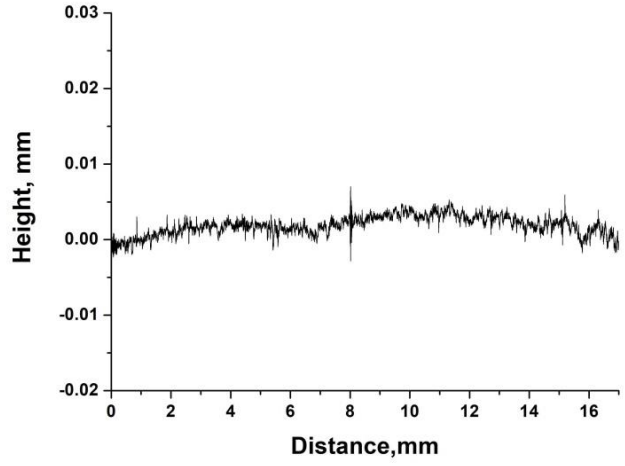

(a)

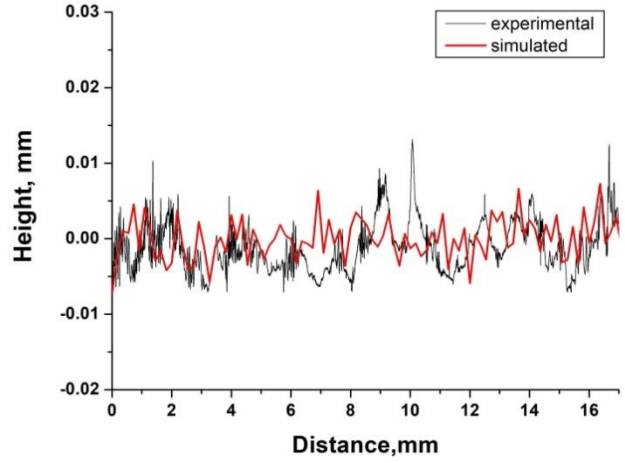

(b)

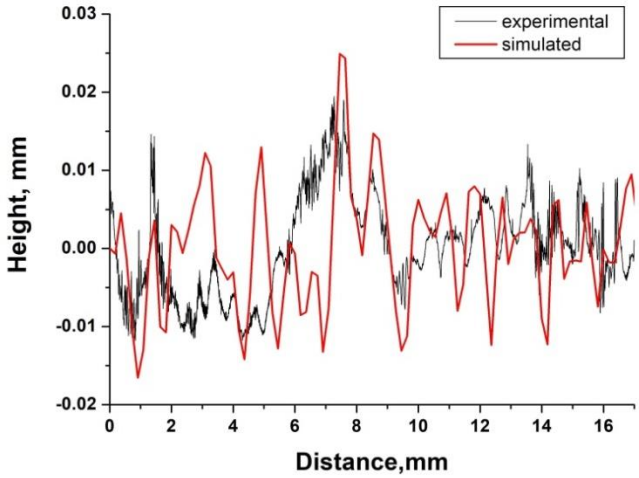

(c)

Figure 4. Surface profile of initial sample (a) and samples treated at Q=37 J/cm^2 with 1 pulse (b) and 3 pulses (c).

3.3. Surface erosion

The hydrodynamic flow of the melt during plasma impact leads to initiation of another process - surface erosion. The study of this process, which occurs under the action of high-temperature plasma flows on materials, is most relevant for studying the processes of plasma disruption and transient processes in ITER. In particular, it was shown in (Tereshin et.al., 2003) that under the action of plasma flows generated by a quasi-steady-state plasma accelerator, a crater is formed on the tungsten surface, onto the edges of which the plasma spreading along the surface squeezes the melt. A similar result was obtained on steel after exposure to compression plasma flows (Leyvi et.al., 2017). Under the conditions of this experiment, the diameter of the plasma spot, depending on the density of the absorbed energy, was 30-45 mm, while the diameter of the research samples was 25 mm. Obviously, if the size of the plasma spot on the plane of the sample surface is larger than the size (diameter) of the sample, then such an effect will lead to the displacement of the melt by the plasma pressure outside the sample.

Hydrodynamic instabilities generated by a plasma flow at the plasma – melt border are also responsible for the melt splashing under the plasma impact assuming corresponding energy density range (Bazylev et.al., 2017; Leyvi et.al., 2017). Perturbations appeared at the surface transformed into ligaments with fine melt droplets that can be stripped from ligament tips and dragged away by the plasma flow (Miloshevsky and Hassanein, 2013). Similar mechanism is considered for the formation of melt droplets and their ejection from surface during pulsed laser action (Brailovsky, 1995).

The results of measurement of samples mass change after plasma impact are shown in Figure 5. It can be seen from the figure that an increase in both the absorbed energy density and the number of pulses lead to the growth of the erosion intensity.

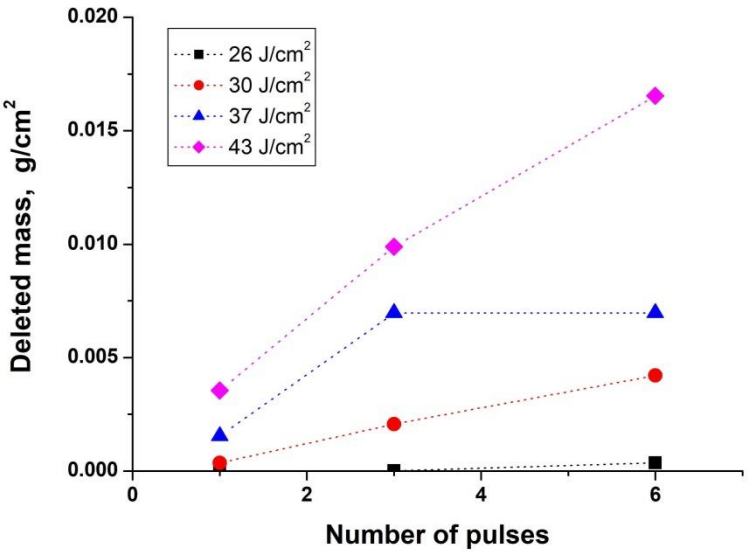

Figure 5. Dependence of the mass deleted from the square unit on n and Q.

The obtained data were averaged over the number of pulses for each value of the absorbed energy density. The resulting dependence of the mass removed per unit area on the density of absorbed energy per pulse is shown in Figure 6. As it can be seen from the figure, the averaged data are well described by the exponential dependence, which was also observed on other materials treated by CPF (Cherenda et.al., 2015).

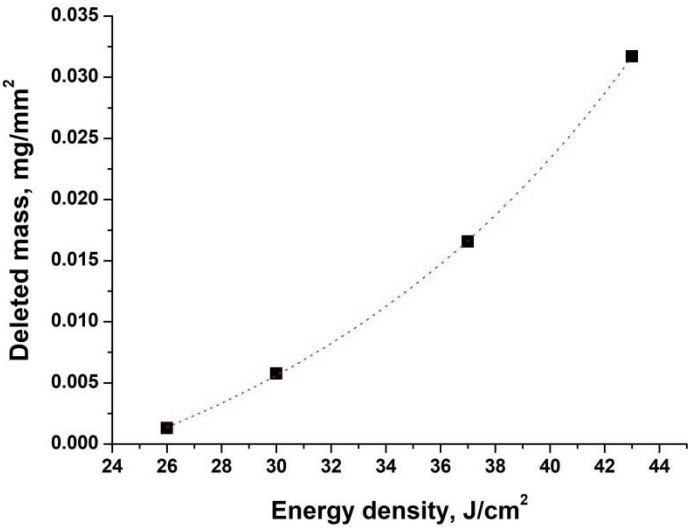

Figure 6. Dependence of the averaged mass deleted from the square unit on Q.

According to the averaged data set the mass (Δm, mg) deleted from the area (S, mm^2) after one plasma pulse at the energy density absorbed by the surface layer (Q, J/cm^2 per pulse) can be find from the following expression (red line in Figure 6):

$$\frac{\Delta m}{S} = 0.00198 \cdot exp\left(\frac{Q}{13.97097}\right) - 0.01136$$

This expression can be used for the samples of Ti-6Al-4V with the size of 25 mm in the used energy density range.

It should also be noted that evaporation, taking into account subsequent condensation, can also made an insignificant contribution to the change in the mass of samples after plasma impact. Another factor that can affect the weight of the sample is the formation of a titanium nitride film on the surface. The formation of a surface film will be discussed below.

3.4. Phase composition

A change in the phase composition of the surface can also affect the resulting surface topography. During CPF generation, nitrogen is injected into the vacuum chamber thus leading to the formation of titanium nitride on the surface as a result of the interaction of gas atoms with the surface heated under plasma impact. Previous studies have shown that the thickness of the nitrided layer is about 1 μm (Cherenda et.al., 2012). It should be noted that due to the high crystallization temperature (~ 2930 ^{o}C for TiN, ~ 1650 ^{o}C for the Ti-6Al-4V alloy), nitride formation can also affect the surface topography. Firstly a change in the elemental composition of the surface will affect the surface tension forces, which tend to smooth out the perturbations of the melt surface formed by the action of hydrodynamic instabilities (Zhang et.al., 2001). Secondly, the crystallizing surface film just after the end of the plasma pulse will prevent the development of melt oscillations. It should be noted that nitride crystallization can also create its own surface relief.

The phase composition investigations carried out by X-ray diffraction analysis confirmed the formation of titanium nitride with a cubic crystal lattice (δ-TiN) on the surface of the alloy under the impact of CPF generated in a nitrogen atmosphere (Figure 7). At the same time, the diffraction peaks of both δ-TiN and α-Ti are shifted to the region of larger angles indicating reduced crystal lattice parameters compared to the standards. In particular, the lattice parameter (a) for δ-TiN determined from the (200) line is 0.4173 nm at n=1, Q=30 J/cm^2 and 0.4153 nm at n=6, Q=30 J/cm^2 (for standard a=0.4241 nm (JCPDS card #38-1420)). This effect is due to the fact that in the initial state the basis of the Ti-6Al-4V alloy is a substitution solid solution α-Ti(Al,V). Since the radii of aluminum and vanadium atoms are smaller than the radius of

titanium atoms, the solid solution of titanium with these elements has smaller crystal lattice parameters. After exposure, the nitride is formed on the basis of this solid solution, i.e. may contain both aluminum and vanadium atoms. Therefore, it would be more correct to assume the formation of a substitution solid solution δ-Ti(Al,V)N.

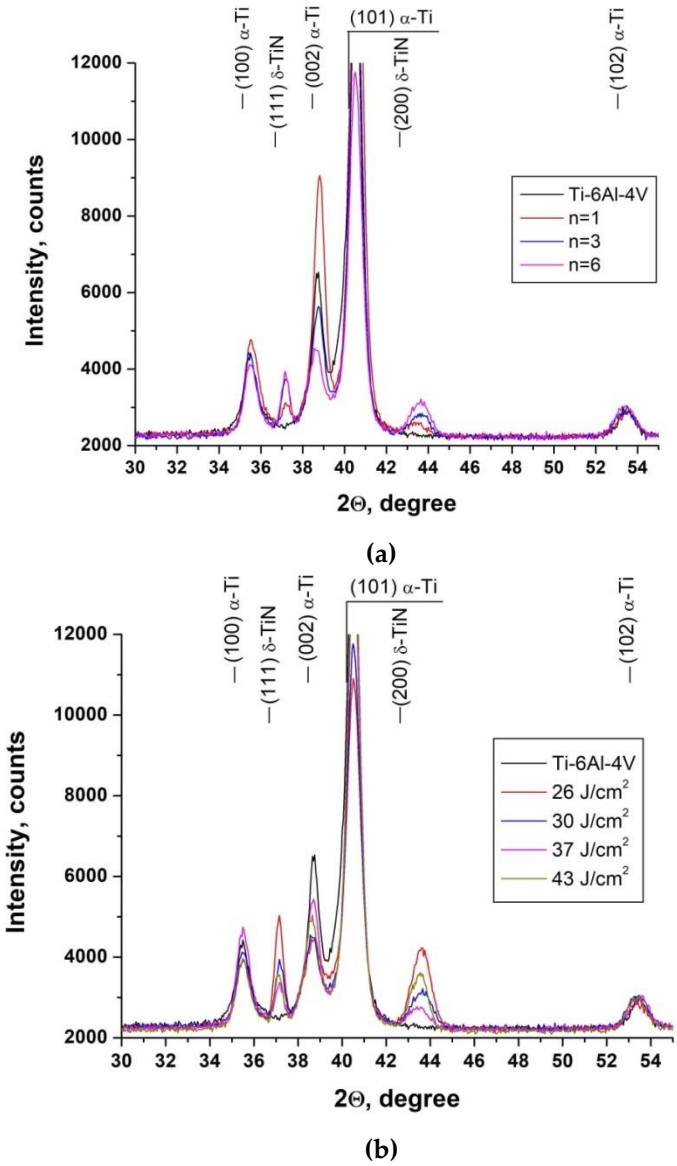

Figure 7. X-ray diffraction patterns of samples treated at 30 J/cm² and different number of pulses (a) and samples treated with 6 pulses and different energy absorbed by the surface layer (b).

The intensity of the nitride diffraction peaks depends on the treatment regimes. An increase in the number of pulses at the same absorbed energy density leads to the growth of the intensity of the (111) δ-TiN and (200) δ-TiN peaks (Figure 7a). Since the intensity of the peaks is proportional to the content of this phase in the analyzed layer, one can speak about growth of the surface nitride film thickness with an increase in the number of pulses. Each subsequent pulse led to the removal of the surface layer containing the nitride film. However, with an increase of pulses number, as it was shown by previous studies (Cherenda et.al., 2020), the surface temperature rises, resulting in the growth of the nitrogen diffusion flux and growth of the nitride film thickness with each subsequent pulse.

A similar tendency is also observed with a decrease in the absorbed energy density (Figure 7b). In particular, this is confirmed by the behavior of the (111) δ-TiN diffraction line intensity. However, it should be noted that there is no similar dependence for the (200) δ-TiN diffraction line. One can say only that the maximum intensity of the δ-TiN diffraction lines is observed for the case of the minimum absorbed energy density - 26 J/cm² (Figure 7b). However, it should be noted that, under conditions of

ultrafast cooling from the melt, texturing of growing grains (growth in certain crystallographic directions) in the surface layer is usually observed, which also affects the intensity of the corresponding diffraction lines. To eliminate this effect, the total intensity of the diffraction lines of titanium nitride (ΣI_{TiN}) and titanium (ΣI_{Ti}) was calculated for each diffraction pattern and their ratio was found. Such a ratio will more correctly and visually reflects the concentration of phases in the analyzed layer. The results are shown in Figure 8. One can see that an increase in the number of pulses for any absorbed energy density (in the range used) leads to an increase in the nitride concentration. With a decrease in the absorbed energy density (at the same number of pulses), the largest increase in the ratio of the total intensity of the phases is observed at a minimum absorbed energy density of 26 J/cm^2.

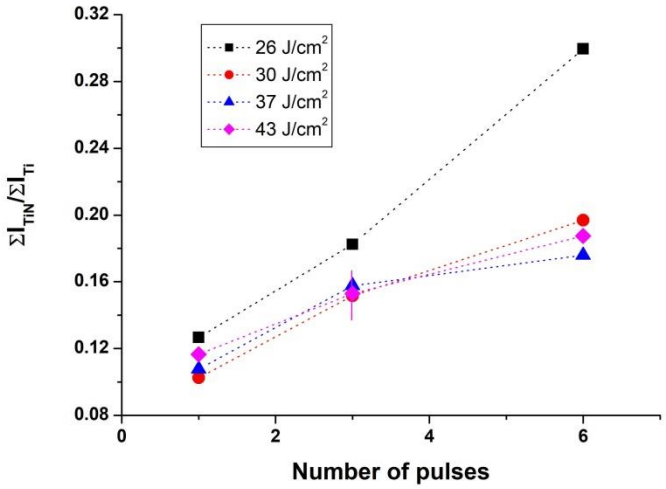

Figure 8. The dependence of $\Sigma I_{TiN}/ \Sigma I_{Ti}$ ratio on on n and Q.

The main reasons for such behavior with a change in the absorbed energy density were considered earlier (Cherenda et.al., 2012). An increase in the absorbed energy leads to an increase in the intensity of evaporation of the material, which forms a shock-compressed layer held directly at the surface of the sample by the oncoming compression plasma flow. This layer prevents the penetration of nitrogen atoms from the atmosphere of the plasma-forming substance into the melt, being a kind of barrier. After the end of the pulse action, the plasma flow compression zone begins to disintegrate, which causes scattering of the shock-compressed layer, filling the near-surface region with nitrogen from the surrounding atmosphere, and creating conditions for efficient diffusion of nitrogen atoms in the material. Thus, the duration of diffusion saturation of the surface layer with nitrogen, which is determined by the time interval between scattering of the shock-compressed layer and cooling of the sample surface to room temperature, decreases with an increase in the absorbed energy density due to an increase in the scattering time of the shock-compressed layer, which explains the decrease of total nitrogen diffusion flux. As a result, the diffusion of nitrogen atoms into the surface layer occurs later and at lower temperatures.

The formation of a titanium nitride film on surface was confirmed by SEM investigations (Figure 9). Surface nitride film possessed dendritic structure due to crystallization in conditions of high cooling speed. No significant changes in structure and dendrites size was found on changing treatment regimes. The formation of nitride film with similar structures was found after alloying of Ti-6Al-4V alloy by copper atoms with CPF (Basalai et.al., 2022).

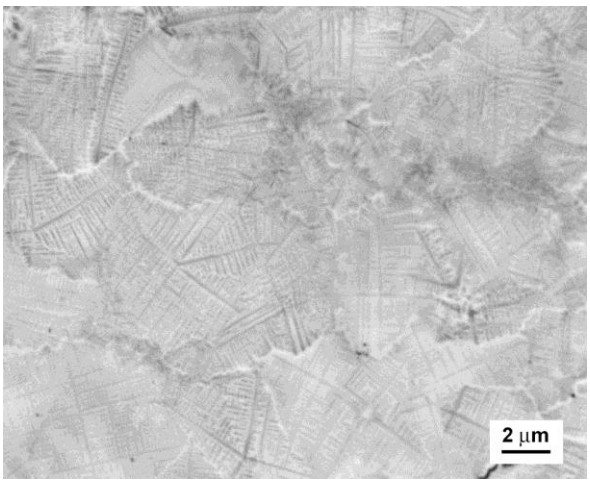

Figure 9. SEM image of samples' surface after CPF treatment at Q = 43 J/cm² and n=3

Investigations of the phase composition of the surface layer showed that the largest volume of titanium nitride (the largest film thickness) is observed at a minimum absorbed energy density of 26 J/cm². Just at this treatment regime it was found that an increase in the number of pulses does not significantly affect the value of R_a parameter (Figure 1a) and leads to a slight increase of W_a parameter (Figure 1d). Thus, one can conclude that the formed titanium nitride film prevents the development of the surface relief initiated by the action of hydrodynamic instabilities.

Besides that surface nitride can play a role of an intermediate layer enhancing adhesion of protective coatings deposited on titanium implants, increase hardness, promote necessary texture, and induce residual stress gradients (Herrera-Jimenez et.al., 2021; Sizova et.al., 2022; Vereschaka et.al., 2019; Grigoriev and Metel, 2004; Vereschaka and Grigoriev et.al., 2020; Grigoriev and Volosova et.al., 2020). In particular, it was shown that preliminary plasma nitriding of Ti-6Al-4V alloy resulted in enhanced adhesion of TiN coating deposited after nitriding (Herrera-Jimenez et.al., 2021). In this case the mechanical properties of protective coating-intermediate layer-substrate system will be strongly dependent on nitrogen content of intermediate layer (Liang et.al., 2023). Investigations carried out showed that nitrogen content as well as volume fraction of δ-TiN are strongly dependent on CPF treatment regimes. Thus investigation of the influence of surface relief and phase composition after plasma impact on mechanical properties and adhesion strength of protective nitride coatings (Grigoriev, Vereschaka, Milovich, Tabakov et.al., 2020; Grigoriev, Vereschaka, Milovich, Sitnikov et.al.; 2020; Vereschaka and Grigoriev et.al., 2021) will be the aim of future experiments.

5. Conclusions

The findings showed that compression plasma flows treatment can be used to form surface relief of Ti-6Al-4V alloy surface with controlled roughness and waviness parameters. In the used range of treatment regimes (number of pulses 1-6, energy absorbed by the surface layer 26-43 J/cm² per pulse) the R_a parameter was changed in the range of 0.7-2.7 μm, R_z – 8-16 μm, R_{max} - 11.3-26.5 μm, and W_a – 1.4- 5.2 μm. Increase of pulses number for Q=30-43 J/cm² resulted in the growth of R_a value, while treatment with minimal Q value of 26 J/cm² did not lead to substantial R_a changes. The behavior of the waviness parameter W_a correlated with the behavior of R_a.

It was shown that hydrodynamic flow of the melt and the appearance of hydrodynamic instabilities at the melt-plasma border are the key factors determining the formation of the resulting surface relief under CPF treatment. The model of the potential flow of an incompressible fluid was used to simulate the relief of the Ti surface under CPF impact. Correlation between simulated and experimental data was found. An increase of pulses number resulted in a smoothing of the short-wavelength part of the surface relief and growth of the long-wavelength part.

The hydrodynamic flow of the melt during plasma impact led to another process - surface erosion. Increase in both the absorbed energy density and the number of pulses resulted in an increase in the erosion intensity. The averaged data of the mass deleted from the surface were well described by the exponential dependence on the energy absorbed by the surface.

Usage of nitrogen as plasma generating gas led to the formation of titanium nitride with a cubic crystal lattice (δ-TiN) as a result of the interaction of gas atoms with the surface heated under plasma impact. Volume fraction of δ-TiN in the analyzed by X-ray layer was strongly dependent on CPF treatment parameters. Increase in the number of pulses or a decrease of the absorbed energy density led to it growth. The largest volume of titanium nitride was observed at a minimum absorbed energy density of 26 J/cm^2. Just at this treatment regime it was found that an increase in the number of pulses did not significantly affect the value of R_a parameter and led to a slight increase of W_a parameter. Thus, the formed titanium nitride film prevents the development of the surface relief initiated by the action of hydrodynamic instabilities.

Acknowledgements

This work (experimental investigations) was supported financially by the Belarusian Republican Foundation for Fundamental Research (project no. T23RNF-228) and the Russian Science Foundation (project no. 23-49-10038).

References

Aparicio, C.; Rodriguez, D.; Gil, F.J.; Variation of roughness and adhesion strength of deposited apatite layers on titanium dental implants. *Materials Science and Engineering C* **2011**, 31, 320-324.

Astashinski, V. M.; Leyvi, A. Ya.; Uglov, V. V.; Cherenda, N. N.; Yalovets, A. P. Formation of Relief on a Metallic Target Surface under the Action of Compression Plasma Flows. *Journal of Surface Investigation. X-ray, Synchrotron and Neutron Techniques* **2014**, 8(3), 519–523.

Basalai, A.V.; Cherenda, N.N.; Petukh, A.B.; Uglov, V.V.; Laskovnev, A.P.; Isobello, A.Yu.; Astashinski, V.M.; Kuzmitski, A.M. The formation of surface Ti-Al-V-Cu alloy by combined ion-plasma treatment. *High Temperature Material Processes* **2022**, 26(1), 33–39.

Bazylev, B.; Janeschitz, G.; Landman, I.; Loarte, A.; Klimov, N.S.; Podkovyrov, V.L.; Safronov, V.M. Experimental and theoretical investigation of droplet emission from tungsten melt layer. *Fusion Engineering and Design* **2009**, 84, 441-445.

Brailovsky, A.B.; Gaponov, S.V.; Luchin, V.I. Mechanisms of melt droplets and solid-particle ejection from a target surface by pulsed laser action. *Appl. Phys. A* **1995**, 61, 81-86.

Bruera, A.; Puddu, P.; Theimer, S.; Villa-Vidaller, M.; List, A.; Bolelli, G.; Gartner, F.; Klassen, T.; Lusvarghi, L. Adhesion of cold sprayed soft coatings: Effect of substrate roughness and hardness. *Surface and Coatings Technology* **2023**, 466, 129651.

Brunello, G.; Brun, P.; Gardin, C.; Ferroni, L.; Bressan, E.; Meneghello, R. Biocompatibility and antibacterial properties of zirconium nitride coating on titanium abutments: An in vitro study. *PLoS ONE* **2018**, 13(6), e0199591.

Chandrasekhar, S. Hydrodynamic and hydromagnetic stability. University Press: Oxford, UK, 1961; 655 p.

Chen, H.; Feng, R.; Xia, T.; Wen, Z.; Li, Q.; Qiu, X.; Huang, B.; Li, Y. Progress in Surface Modification of Titanium Implants by Hydrogel Coatings. *Gels* **2023**, 9, 423.

Chen, Q.;. Thouas, G. A. Metallic implant biomaterials. *Mater. Sci. Eng. R* **2015**, 87, 1–57.

Cherenda, N.N.; Basalai, A.V.; Shymanski, V.I.; Uglov, V.V.; Astashynski, V.M.; Kuzmitski, A.M.; Laskovnev, A.P.; Remnev, G.E. Modification of Ti-6Al-4V alloy element and phase composition by compression plasma flows impact. *Surface & Coatings Technology* **2018**, 355C, 148-154.

Cherenda, N. N.; Laskovnev, A. P.; Basalai, A. V.; Uglov, V. V.; Astashynski, V. M.; Kuzmitski, A. M. Erosion of Materials under the Effect of Compression Plasma Flows. *Inorganic Materials: Applied Research* **2015**, 6 (2), 114–120.

Cherenda, N.N.; Shimanskii, V. I.; Uglov, V. V.; Astashinskii, V. M.; Ukhov, V. A. Nitriding of Steel and Titanium Surface Layers under the Action of Compression Plasma Flows. *Journal of Surface Investigation. X-ray, Synchrotron and Neutron Techniques* **2012**, 6(2), 319-325.

Cherenda, N.N., Uglov, V.V., Martinovich, Yu.V.; Betanov, I.A.; Astashynski, V.M.; Kuzmitski, A.M. Structure of the austenitic steel surface layer subjected to compression plasma flows. impact. *High Temperature Material Processes* **2020**, 24(3), 211–225.

Chouirfa, H.; Bouloussa, H.; Migonney, V.; Falentin-Daudré, C. Review of titanium surface modification techniques and coatings for antibacterial applications. *Acta Biomaterialia* **2019**, 83, 37- 54.

Croll, S.G.; Surface roughness profile and its effect on coating adhesion and corrosion protection: A review. *Progress in Organic Coatings* **2020**, 148, 105847.
Grabovetskaya, G. P.; Stepanova, E. N.; Zabudchenko O. V.; Mishin, I. P. Formation of the Structure and Properties of the Near-Surface Layer in Alloys of the Ti–6Al–4V–H System Under Irradiation with a Pulsed Electron Beam. *Russian Physics Journal* **2023**, 66, 172–179.
Grigoriev, S.; Metel, A. Plasma- and beam-assisted deposition methods. Nanostruc. *Thin Films Nanodisper. Strength. Coat.* **2004**, 155, 147-154.
Grigoriev, S.N.; Volosova, M.A.; Vereschaka, A.A.; Sitnikov, N.N.; Milovich, F.; Bublikov, J.I.; Fyodorov, S.V.; Seleznev, A.E. Properties of (Cr,Al,Si)N-(DLC-Si) composite coatings deposited on a cutting ceramic substrate. *Ceram. Int.* **2020**, 46, 18241–18255.
Grigoriev, S.; Vereschaka, A.; Milovich, F.; Tabakov, V.; Sitnikov, N.; Andreev, N.; Sviridova, T. Bublikov, J. Investigation of multicomponent nanolayer coatings based on nitrides of Cr, Mo, Zr, Nb, and Al. *Surf. Coat. Technol.* **2020**, 401, 126258.
Grigoriev, S.; Vereschaka, A.; Milovich, F.; Sitnikov, N.; Andreev, N.; Bublikov, J.; Kutina, N. Investigation of the properties of the Cr,Mo-(Cr,Mo,Zr,Nb)N-(Cr,Mo,Zr,Nb, Al)N multilayer composite multicomponent coating with nanostructured wear-resistant layer. *Wear* **2021**, 468, 203597.
Herrera-Jimenez, E.J.; Bousser, E.; Schmitt, T.; Klemberg-Sapieha, J.E.; Martinu, L. Effect of plasma interface treatment on the microstructure, residual stress profile, and mechanical properties of PVD TiN coatings on Ti-6Al-4V substrates. *Surface and Coatings Technology* **2021**, 413, 127058.
Kaur, M.; Singh, K. Review on titanium and titanium based alloys as biomaterials for orthopaedic applications. *Materials Science & Engineering C* **2019**, 102, 844-862.
Khorasani, A.M.; Goldberg, M.; Doeven, E.H.; Littlefair, G. Titanium in Biomedical Applications - Properties and Fabrication: a Review. *Journal of Biomaterials and Tissue Engineering* **2015**, 5, 593–619.
Konovalov, S.; Chen, X.; Sarychev, V.; Nevskii, S.; Gromov V.; Trtica M. Mathematical Modeling of the Concentrated Energy Flow Effect on Metallic Materials. *Metals* **2017**, 7, 4.
Krasnikov, V.S.; Leivy, A.Y.; Mayer, A.E.; Yalovets, A.P. Surface microrelief smoothing mechanisms in a target irradiated by an intense charged particle beam. *Rus. J. Tech. Physics* **2007**, 52(4), 431.
Kurup, A.; Dhatrak, P.; Khasnis, N. Surface modification techniques of titanium and titanium alloys for biomedical dental applications: A review. *Materials Today: Proceedings* **2021**, 39(1), 84-90.
Leyvi, A.Ya. Study of parameters of a facility generating compressive plasma flows. *IOP Journal of Physics: Conference Series* **2017**, 830, 012065.
Leyvi, A.Ya.; Cherenda, N.N.; Uglov, V.V.; Yalovets, A.P. The impact of a shock-compressed layer on the mass transfer of target material during processing compression plasma flows. *Resource-Efficient Technologies* **2017**, 3, 222–225.
Liang D.; Dai, W. Effect of Nitrogen Partial Pressure on Structure, Mechanical Property, and Corrosion Behavior of ZrNx Films Prepared by Reactive DC Magnetron Sputtering. *Scanning* **2023**, 2023, 3604077.
Liu, H.; Liu, R.; Ullah, I.; Zhang, S.; Sun, Z.; Ren, L.; Yang, K. Rough surface of copper-bearing titanium alloy with multifunctions of osteogenic ability and antibacterial activity. *Journal of Materials Science & Technology* **2020**, 48, 130–139
Lu, A.; Gao, Y.; Jin, T.; Luo, X.; Zeng, Q.; Shang, Z. Effects of surface roughness and texture on the bacterial adhesion on the bearing surface of bio-ceramic joint implants: An in vitro study. *Ceramics International* **2020**, 46, 6550-6559.
Lu, M.; Zhang, Z.; Zhang, J.; Wang, X.; Qin, G.; Zhang, E. Enhanced antibacterial activity of Ti-Cu alloy by selective acid etching. *Surface & Coatings Technology* **2021**, 421, 127478.
Lüdecke, C.; Bossert, J.; Roth, M.; K.; Jandt, D. Physical vapor deposited titanium thin films for biomedical applications: reproducibility of nanoscale surface roughness and microbial adhesion properties. *Applied Surface Science* **2013**, 280, 578-589.
Miloshevsky, G.; Hassanein, A. Splashing and boiling mechanisms of melt layer losses of PFCs during plasma instabilities. *Journal of Nuclear Materials* **2013**, 438, S155-S159.
Nevskii, S.; Sarychev, V.; Konovalov, S.; Granovskii A.; Gromov, V. Formation Mechanism of Micro- and Nanocrystalline Surface Layers in Titanium and Aluminum Alloys in Electron Beam Irradiation. *Metals* **2020**, 10, 1399.
Nouri, A.; Wen C. Introduction to surface coating and modification for metallic biomaterials. In Surface Coating and Modification of Metallic Biomaterials. 1st Ed.; Cuie Wen; Woodhead Publishing, Cambridge, UK, 2015; pp. 3-60.
Padmini, B.V.; Niranjan, H.B.; Kumar, R.; Padmavathi, G.; Nagabhushana, N.; Mohan, N. Influence of substrate roughness on the wear behaviour of kinetic spray coating. *Materials Today: Proceedings* **2020**, 27(3), 2498-2502.
Robles, D.; Brizuela, A.; Fernández-Domínguez, M.; Gil, J. Corrosion Resistance and Titanium Ion Release of Hybrid Dental Implants. *Materials* **2023**, 16, 3650.
Sachin, P.G.; Uppoor, A.S.; Nayak, S.U.; Nano-scale surface modification of dental implants – An emerging boon for osseointegration and biofilm. *Control Acta Marisiensis - Seria Medica* **2022**, 68(4), 154-158.

Sarychev, V. D.; Mochalov, S. P.; Budovskikh, E. A.; Vashchuk, E. S.; Gromov, V. E. Formation of Convective Structures in Metals and Alloys under the Action of Pulsed Multiphase Plasma Jets. *Steel in Translation* **2010**, 40(6) 531–536.

Simões, I. G.; Reis, A. C.; Valente, M. L. C. Influence of surface treatment by laser irradiation on bacterial adhesion on surfaces of titanium implants and their alloys: Systematic review, *The Saudi Dental Journal* **2023**, 35(2), 111-124.

Sizova, O. V.; Teryukalova, N. V.; Leonov, A. A.; Denisova, Yu. A.; Novitskaya O. S., A. Kolubaev, V. Influence of the intermediate layer on the adhesion and friction of titanium-based nitrided coatings on a copper substrate. *Russian Physics Journal* **2022**, 65(7), 1123-1129.

Steinmann, P.A.; Tardy, Y.; Hintermann, H.E. Adhesion testing by the scratch test method: The influence of intrinsic and extrinsic parameters on the critical load. *Thin Solid Films* **1987**, 154, 1987, 333-349.

Subramanian, C.; Strafford, K.N.; Wilks, T.P.; Ward, L.P.; McMillan, W. Influence of substrate roughness on the scratch adhesion of titanium nitride coatings. *Surface and Coatings Technology* **1993**, 62, 529-535.

Takadoum, J.; Bennani, H. H. Influence of substrate roughness and coating thickness on adhesion, friction and wear of TiN films. *Surface and Coatings Technology* **1997**, 96, 272-282.

Tardelli, J. D. C.; Firmino, A. C. D.; Ferreira, I.; Reis A.C. Influence of the roughness of dental implants obtained by additive manufacturing on osteoblastic adhesion and proliferation: A systematic review. *Heliyon* **2022**, 8(12), e12505.

Tereshin, V.I.; Garkusha, I.E.; Bandura, A.N.; Byrka, O.V.; Chebotarev, V.V.; Makhlaj, V.A.; Solyakov, D.G.; Wuerz, H. Influence of plasma pressure gradient on melt layer macroscopic erosion of metal targets in disruption simulation experiments. *Journal of Nuclear Materials* **2003**, 313–316, 685–689.

Truong, V. K.; Lapovok, R.; Estrin, Y. S.; Rundell, S.; Wang, J. Y.; Fluke, C. J.; Crawford, R. J.; Ivanova, E.P. The influence of nano-scale surface roughness on bacterial adhesion to ultrafine-grained titanium. *Biomaterials* **2010**, 31, 3674-3683.

Uglov, V.V.; Anishchik, V.M.; Astashynski, V.V.; Astashynski, V.M.; Ananin, S.I.; Askerko, V.V.; Kostyukevich, E.A.; Kuz'mitski, A.M.; Kvasov, N.T.; Danilyuk, A.L.; The effect of dense compression plasma flow on silicon surface morphology. *Surface and Coatings Technology* **2002**, 158 –159, 273–276.

Vereschaka, A.; Grigoriev, S.; Tabakov, V.; Migranov, M.; Sitnikov, N.; Milovich, F.; Andreev. N. Influence of the Nanostructure of Ti-TiN-(Ti,Al,Cr)N Multilayer Composite Coating on Tribological Properties and Cutting Tool Life. *Tribol. Int.* **2020**, 150, 106388.

Vereschaka, A.; Tabakov, V.; Grigoriev, S.; Sitnikov, N.; Milovich, F.; Andreev, N.; Bublikov, J. Investigation of wear mechanisms for the rake face of a cutting tool with a multilayer composite nanostructured Cr–CrN-(Ti,Cr,Al,Si)N coating in high-speed steel turning. *Wear* **2019**, 438-439, 203069.

Vereschaka, A.; Grigoriev, S.; Milovich, F.; Sitnikov, N.; Migranov, M.; Andreev, N.; Bublikov, J.; Sotova, C. Investigation of tribological and functional properties of Cr,Mo-(Cr,Mo) N-(Cr,Mo,Al)N multilayer composite coating. *Tribol. Int.* **2021**, 155, 106804.

Wang, Q.; Zhou, P.; Liu, S.; Attarilar, S.; Ma, R. L.-W.; Zhong Y.; Wang, L. Multi-Scale Surface Treatments of Titanium Implants for Rapid Osseointegration: A Review. *Nanomaterials* **2020**, 10, 1244.

Wu, N.; Gao, H.; Wang, X.; Pei, X. Surface Modification of Titanium Implants by Metal Ions and Nanoparticles for Biomedical Application. *ACS Biomater. Sci. Eng.* **2023**, 9(6), 2970–2990.

Yang, K.; Shi, J.; Wang, L.; Chen, Y.; Liang, C.; Yang, L.; Wang, L.-N. Bacterial anti-adhesion surface design: Surface patterning, roughness and wettability: A review. *Journal of Materials Science & Technology* **2022**, 99, 82-100.

Zhang, R.; He, X.; Doolen, G.; Chen, S. Surface tension effects on two-dimensional two-phase Kelvin-Helmholtz instabilities. *Advances in Water Resources* **2001**, 24, 461-478.

Zhang, W.; Zhang, S.; Liu, H.; Ren, L.; Wang Q.; Zhang, Y.; Effects of surface roughening on antibacterial and osteogenicproperties of Ti-Cu alloys with different Cu contents. *Journal of Materials Science & Technology* **2021**, 88, 158–167.